

Supplemental Material for:

“Experimental test of an expression for the decay of an autocorrelation function”

Journal: Physical Review Letters

Authors: Zach Haralson and J. Goree

I. Experimental setup

The vacuum chamber and optics were previously described in Ref. [1]. Here we present further details, especially of the optics, shown in Fig. SM1.

Laser beams were used for two purposes: illumination and manipulation. There were three main beam lines, one for illumination using a 577 nm laser and two for laser heating manipulation using a 532 nm laser. For these three beam lines, the laser beams were each directed into the chamber by a pair of mirrors called “scanning mirrors.” Within each pair, one mirror provided scanning along an x axis, and the other along a y axis.

For illumination, a laser beam that passed through the optics labeled in Fig. SM1 was formed into a fan of light that shone on the entire collection of microspheres inside the chamber. The scanning mirrors for the illumination beam line, Fig. SM2, were held at constant positions so that the fan of light remained steady and did not move.

Similar optics were used in the two beam lines for laser heating, except that these beam lines did not include a negative cylindrical lens. The scanning mirrors for these beam lines moved according to an applied voltage waveform, as described in [2].

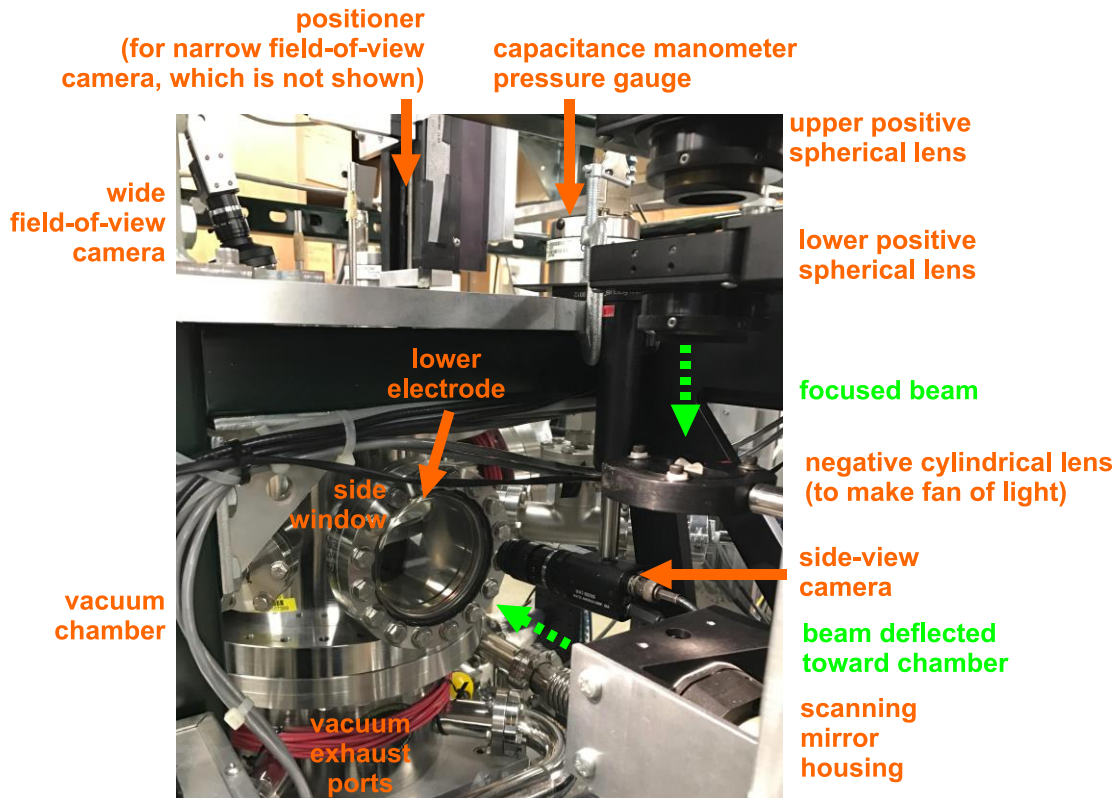


FIG. SM1. Photograph of vacuum chamber and optical components. The beam indicated here is the one that is shaped into a fan and used to illuminate the polymer microspheres.

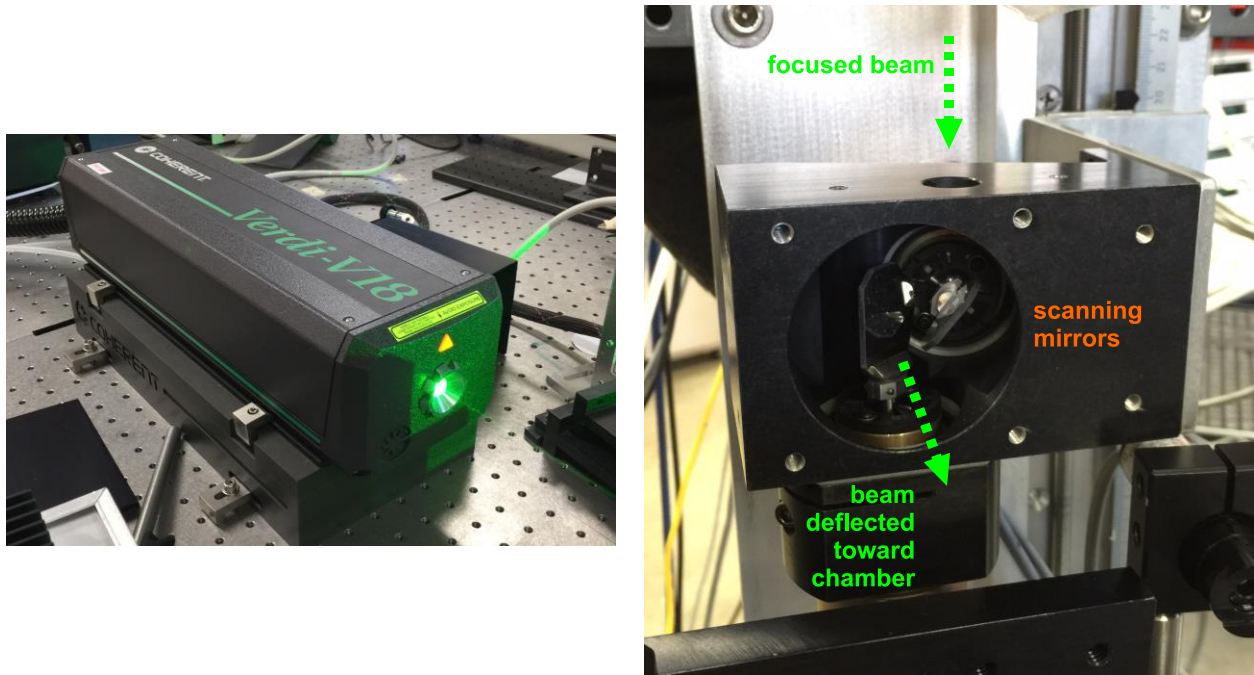


FIG. SM2. Photographs of 18-W laser for laser heating manipulation (left) and scanning mirror housing assembly (right).

For the experimental runs described in the main text and in this Supplemental Material, the only laser manipulation used was heating. Our apparatus, as described in [1], also included a pair of beam lines for shear manipulation, but we did not use these for the runs analyzed here. In other words, in this Letter we analyze only the runs with conditions that mimic an equilibrium, with no macroscopic flows or gradients. The laser and optics for the shear manipulation are not shown here.

II. Fits of ACFs from other experimental runs

We calculated experimental autocorrelation functions (ACFs) for eight runs under liquid conditions. The two runs we presented in Fig. 2 of the main text were the ones that exhibited the most severe and least severe failure for an exponential. The experimental ACFs and their fits from the other six runs are shown in Figs. SM3 and SM4.

Results from all six of these runs show the same main features as the two runs presented in Fig. 2 of the main text: the expression of BC fits the experimental ACF data well over the entire time range, while the exponential fit fails, especially at short time.

As a minor point, we note that for the runs with high temperatures, noise tended to dominate the experimental ACFs sooner than for the other runs. For this reason, we present the ACF data for a shorter time range in Fig. SM4, and correspondingly we also perform our fits (to both functions) over only the time range shown for these runs.

Values of $C(0)$ are tabulated for all eight liquid runs in Table I. Following a common practice, in our plots of the ACF we have normalized $C(t)$ by $C(0)$ so that the curves all begin at unity.

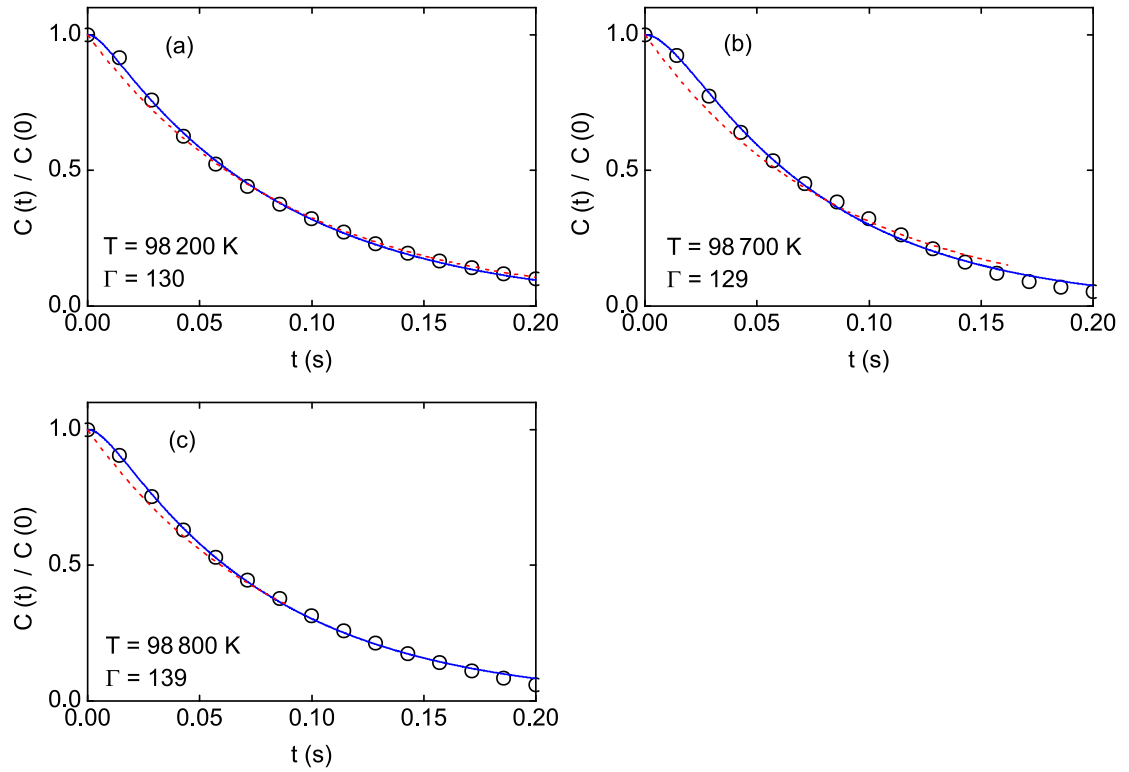


FIG. SM3. Shear stress ACFs from three low temperature runs. As in Fig. 2 of the Letter:

- Experimental ACFs are shown as data points
- Fit to Eq. (1) of the Letter is shown as a solid line
- Fit to an exponential decay is shown as a dashed line

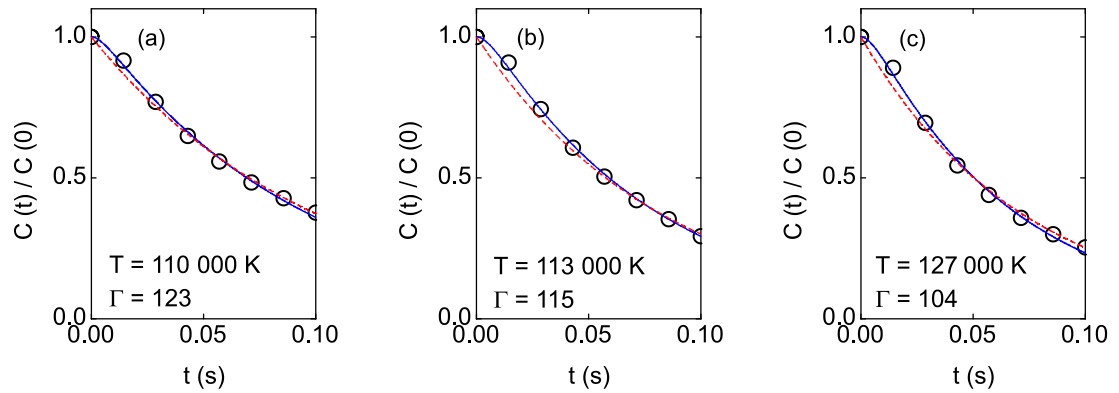


FIG. SM4. Shear stress ACFs from three high temperature runs.

TABLE I. Initial values of the shear stress ACF for each experimental run.

Figure Panel	$C(0)$ ($10^{-31} \text{ kg}^2 \text{ m}^4 / \text{s}^4$)
2(a) of Letter	3.31
2(b) of Letter	3.49
SM3(a)	3.49
SM3(b)	3.38
SM3(c)	3.95
SM4(a)	3.55
SM4(b)	3.22
SM4(c)	3.23

III. Physical interpretation of the transition in the shape of the ACF decay

As we mention in the main text, Belousov and Cohen \cite{belousov.2016} did not present an intuitive interpretation of the shape of the ACF decay when they reported their theory. Here we suggest as an interpretation that the transition is due to the accumulation of collisional scattering. This interpretation is supported by our finding that a change, at approximately the same time as the transition in the ACF, is observed in two other kinds of data.

First, particle-tracking data in Fig. 1 shows trajectories that appear to be straight for the first few data points, and then become deflected. The microsphere trajectories are all deflected in different directions at different times, as would be expected for a microscopic stochastic process. Physically, we can describe the straight and deflected portions of trajectories as the signatures of ballistic motion and collisional scattering, respectively. Since most of the trajectories become deflected by about $\omega_{pd} t \cong 4$ or 5, in dimensionless units, we can identify this range as the typical time scale for the accumulation of collisional scattering. Moreover, we note that this time scale coincides with the transition seen in the ACF which is generally in the range $3 < \omega_{pd} t < 7$.

Second, our data exhibit a well-known transition in the diffusion curve, which is a plot of mean-square-displacement (MSD) versus time. This curve exhibits a distinctive power-law scaling $\text{MSD} \propto t^2$ at early times for ballistic motion, which succumbs at later times to a scaling closer to $\text{MSD} \propto t^1$ for diffusive motion.

An experimental diffusion curve is shown in Fig. SM5(a), using data from same run as in Fig. 2(a) of the main text.

As expected, the experimental diffusion curve results exhibit different power-law scalings at short and long times. Solid lines show that at early times the MSD is proportional to t^2 , while at later times the MSD is more nearly proportional to t^1 . The crossing point of these lines at $\omega_{pd} t = 4.4$ identifies the transition from ballistic motion to diffusive motion in the collection of microspheres.

The coincidence of this transition in the MSD curve, as compared to the transition in the ACF data from the same experimental run, lends confidence to the intuitive description we proposed in the main text.

To provide supporting data, we also compare to a simulation performed by our collaborator Bin Liu, using conditions that matched the experimental run. The simulation was a Langevin molecular dynamics simulation of 4096 particles, which were constrained to move in a 2D plane and interacted with a Yukawa potential. The parameters of the simulation were chosen to match those of the experimental run, with $\Gamma = 123$, $\kappa = 0.74$, $\omega_{pd} = 88 \text{ s}^{-1}$, and a gas friction coefficient of 1.1 s^{-1} , as expected for argon at 6 mTorr [3]. The result of the simulation is the MSD curve in Fig. SM5(b), which is very similar to the experimental curve. The transition in

the simulation MSD curve occurred at $\omega_{pd} t = 3.3$, which is close enough to the experimental result to indicate that the physics included in the simulation, including the stochastic particle motion, is adequate to explain the experimentally observed transition from ballistic to diffusive motion.

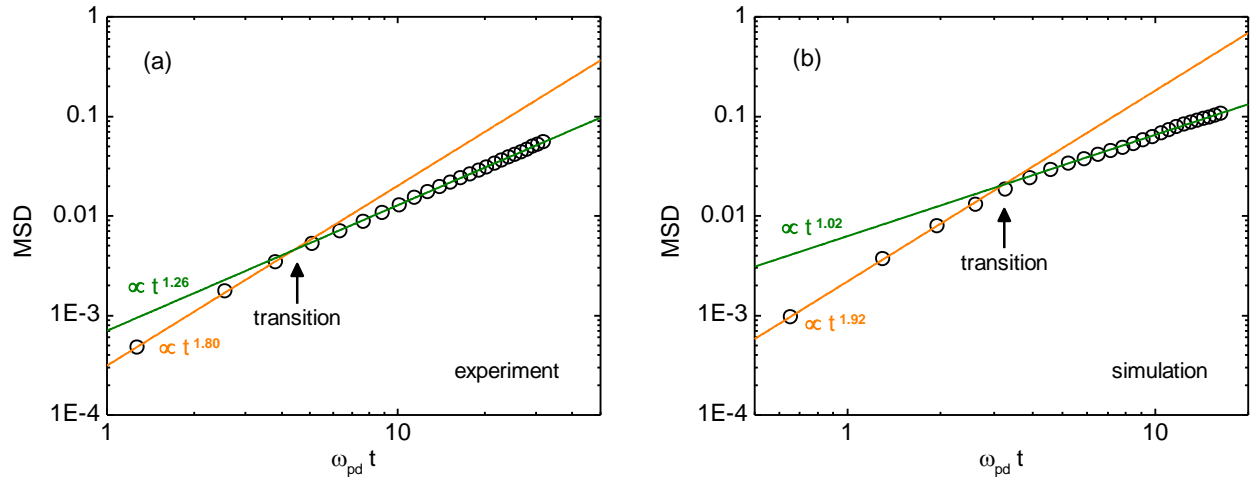


FIG. SM5. Diffusion curves for (a) an experimental run and (b) a simulation performed with conditions that mimic the experiment. The orange and green solid lines are power-law fits to the data at early and late times, respectively. Note that time is shown in dimensionless units, and both axes are logarithmic.

References:

- [1] Z. Haralson and J. Goree, *Phys. Plasmas* **23**, 093703 (2016).
- [2] Z. Haralson and J. Goree, *IEEE Trans. Plasma Sci.* **44**, 549 (2016).
- [3] B. Liu, J. Goree, V. Nosenko, and L. Boufendi, *Phys. Plasmas* **10**, 9 (2003).